

Design and Analysis of a Triple-band Non-zonal Polarization Electromagnetic Metamaterial Absorber

Han Wu, Shijun Ji*, Ji Zhao, Zhiyou Luo, and Handa Dai

School of Mechanical and Aerospace Engineering, Jilin University, Changchun, 130025, China
 hwu19@mails.jlu.edu.cn, jishijun@126.com*, jzhao@jlu.edu.cn, zyluo19@mails.jlu.edu.cn, dhd@jlu.edu.cn

Abstract — A facile design of a novel triple-band electromagnetic metamaterial absorber (MMA) with polarization insensitive property is proposed in this paper. Each unit of the MMA consists of upper copper resonator and bottom copper plate with middle dielectric FR-4 between them. The MMA performs three absorption peaks at 16.919 GHz, 21.084 GHz and 25.266 GHz with absorption rates 99.90%, 97.76% and 99.18%, respectively. The influence of the main structural parameters on the frequencies and absorption rates is analyzed. The absorption mechanism of the absorber is explained by electric field, magnetic field and surface current distributions, which is supported by the electromagnetic parameters, affected with magnetic resonance. The polarization-insensitivity of TE wave is verified by observing the effects of the polarization angle change from 0-90°. The MMA can be applied in radiation, spectrum imaging detector, electromagnetic wave modulator, and so on.

Index Terms — Electromagnetic metamaterials, polarization-insensitive, resonator, triple-band.

I. INTRODUCTION

Metamaterial is a kind of composite material with subwavelength structure, it has some special physical property which doesn't possess by other nature materials [1, 2]. The composites that own man-made structure can be an important material for the manufacture of electromagnetic wave absorption instruments due to geometrical structure parameters and material properties of the metamaterials can be adjusted. In the 2008, Landy [3] proposed a design concept of electromagnetic wave metamaterial absorber (MMA) for the first time, scholars are beginning to become increasingly interested in using artificial metamaterials to pursue near-perfect absorbers. In recent years, MMA research has gradually spread to the physical, informational and engineering fields. Until now, its potential application has expanded to different industries, such as stealth material [4], super lens [5], sensor [6, 7], thermal imaging instrument [8] and so on [9, 10]. The excellent performance has been shown in

single-band [11-15], dual-band [16-20], multi-band [21-23] and broadband operations [24-27].

In some microwave ranges, multi-band MMA has also appeared frequently in recent studies. The metamaterials have some unique electromagnetic properties, which can be constructed by human design. Jianping Xu et al [28] propose a three-band metamaterial absorber, its absorption peaks are 4.36 GHz, 8.41 GHz and 14.67 GHz, three peaks absorption rates are 99.8%, 97.4% and 99.9% respectively. Nguyen et al. [29] analyzed the causes of polarization insensitivity, with two absorption peaks at 10.15 GHz and 10.50 GHz and the absorption rate of around 96.5%. A bandwidth-enhanced microwave absorber using a resonant metamaterial is presented by Lee et al. [30]. They obtained two absorption peaks at 9.8 GHz and 10.3 GHz, and the absorption rate were 99% and 98%, respectively. Li et al. [21] proposed a new metamaterial absorber with a tetra-arrow resonator (TAR) structure, two absorption peaks operating at 6.16 GHz and 7.9 GHz can be obtained, whose absorptivity came up to 99%. A triple-band metamaterial absorber was presented by Huang et al. [23], the proposed absorber can perform absorption peaks at three resonant frequencies 9.86 GHz, 12.24 GHz and 15.34 GHz with the absorption of 99.4%, 96.7% and 99.1%, respectively. Bian et al. [31] designed and fabricated a novel triple-band polarization-insensitive wide-angle ultra-thin microwave metamaterial absorber, it shows three distinctive perfect absorption peaks at frequencies of 3.07 GHz, 5.65 GHz and 8.11 GHz with absorption rates 99.87%, 99.98% and 99.99%, respectively. A new kind of multi-band metamaterial absorber based on the concentric ring resonators is engineered by Gunduz et al. [32] with the absorption peak of 5.98 GHz and 11.12 GHz, and the absorption rate were 99.16% and 99.95%. Shen et al. [33] designed a microwave triple-band metamaterial absorber with three absorption peaks of 99% at 4.06 GHz, 93% at 6.73 GHz and 95% at 9.22 GHz respectively. However, the absorption peaks of the above absorbers are all below the K-band, and the surface structure is relatively sophisticated, and not all peaks are perfect in terms of

absorption performance.

In this paper, a three-layer structure was used to design the triple-band MMA, which consists of top copper three-fork resonator and bottom copper plate with medium FR-4. Through a large amount of simulation, it can be obtained that this absorber has three absorption peaks of 99.90% at 16.919 GHz, 97.76% at 21.084 GHz and 99.18% at 25.266 GHz, respectively. The MMA has higher absorption rates: the absorption rates of the first and third peaks are over 99.18%, and the absorption rate of the second peak is close to 98%. In addition, the distribution of electromagnetic field and surface current is analyzed in detail, and the polarization insensitivity of the absorber is verified by observing the effect of the polarization angle change on absorption. In order to obtain the outstanding absorption rates, the thickness of dielectric layer and the dimension of unit-cell structure were iteratively optimized by using electromagnetic simulation software, and analyzed how these changes in parameters interfere in the absorption peaks.

II. ABSORPTION MECHANISM

The metamaterials absorbent apparatus has the sub-wavelength characteristic, which is composed of the periodic arrangement of the unit structure, and its resonance characteristics are mainly determined by the geometrical parameters of the unit structure, such as pattern shape, dimension and arrangement, as well as the electromagnetic parameters of each layer, so the reasonable optimization design unit structure in a certain frequency range can realize the effective regulation of the resonant frequency.

In order to achieve perfect absorption, the metamaterial absorber should generally meet two basic requirements: Firstly, the structure of the design unit is optimized so that the equivalent input impedance is matched with the free space impedance [34]. Second, it is required that the metamaterial structure has a sufficiently large imaginary part of the dielectric constant and the magnetic permeability to satisfy the electromagnetic wave can be absorbed as soon as possible after entering the metamaterial structure. To prevent transmission, the bottom layer is covered with a metal film so that $T(\omega) = 0$.

When the electromagnetic wave is normally incident to the surface of the metamaterial structure, retrieved electromagnetic parameters of the metamaterial can be calculated according to the definition of S parameter [34, 35]. The reflection rate and transmission rate were: $R(\omega) = |S_{11}|^2$ and $T(\omega) = |S_{21}|^2$, absorption rate of corresponding metamaterial $A(\omega)$ can be expressed by Equation (1):

$A(\omega) = 1 - R(\omega) - T(\omega) = 1 - |S_{11}|^2 - |S_{21}|^2$. (1)
For S_{21} with a thickness of d , which can be expressed by Equation (2):

$$S_{21}^{-1} = \left[\sin(nkd) - \frac{i}{2} \left(z + \frac{1}{z} \right) \cos(nkd) \right] e^{ikd}. \quad (2)$$

Where, $n = n_1 + in_2$ is the complex refractive index of the metamaterial. $z = z_1 + iz_2$ is complex impedance. $k = \omega/c$ is the number of transmission waves in the metamaterial, c is the speed of light.

The reflectivity $R(\omega)$ and transmittance $T(\omega)$ of the electromagnetic wave in the metamaterial can be written as following Equation (3) and Equation (4):

$$\lim_{Z(\omega)=1} R(\omega) = |S_{11}|^2 = \left[\frac{Z(\omega) - 1}{Z(\omega) + 1} \right]^2 = 0, \quad (3)$$

$$\begin{aligned} \lim_{n_2 \rightarrow \infty} T(\omega) &= |S_{21}|^2 = \lim_{n_2 \rightarrow \infty} (e^{-i(n_1-1)kd} \cdot e^{n_2kd}) \\ &= \lim_{n_2 \rightarrow \infty} e^{-2n_2kd} = 0. \end{aligned} \quad (4)$$

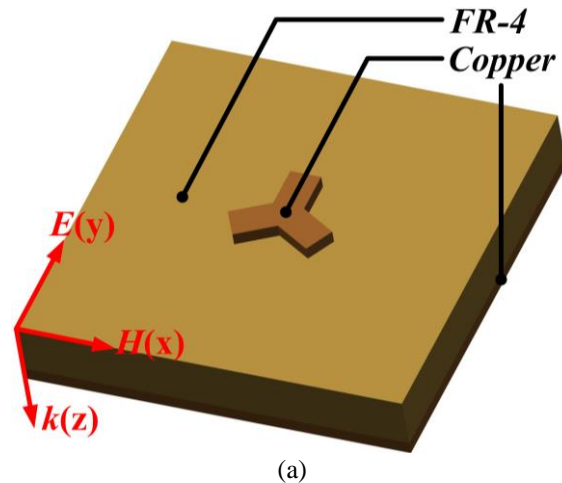
Then the absorption rate of the $A(\omega)$ can be calculated by Equation (5):

$$A(\omega) = 1 - R(\omega) - T(\omega) = 1. \quad (5)$$

According to the above analysis, when the impedance of the metamaterial absorber matches the impedance of the free space [37], that is $Z(\omega) = 1$, only a little proportion of electromagnetic waves are reflected, almost all waves enter the micro-structures of the metamaterial and finally lost.

III. DESIGN AND SIMULATION

The proposed MA structure is composed of the combination of three same size and shape elongated patch resonators as shown in Fig. 1. It consists of the three-layer as described above with copper membranes of the top and bottom layers. The material of the middle layer is FR-4. After geometrical optimization, the optimal structural parameters of the unit cell are obtained as follows: $p=15$ mm, $t_1=0.018$ mm, $a=0.6$ mm, $b=2$ mm, $t_2=1.2$ mm, $t_3=0.018$ mm. $\sigma=5.96 \times 10^7$ S/m is the electric conductivity of copper and $\epsilon_r=4.3$ is the electric permittivity of dielectric spacer, corresponding to the loss tangent $\tan(\delta)=0.025$.



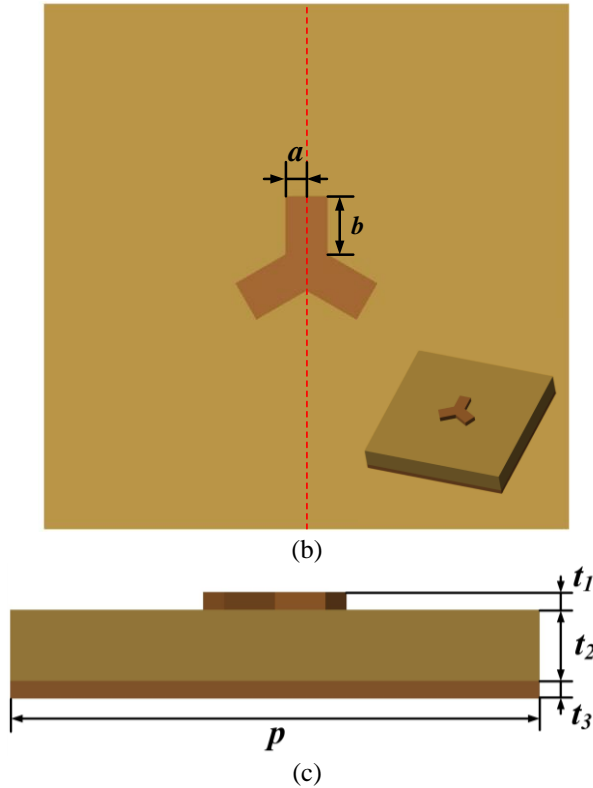


Fig. 1. The structure of the proposed MMA: (a) perspective view of the unit cell, (b) top view, and (c) side view.

The electromagnetic characteristics of the MMA are designed and analyzed by an electromagnetic software CST. The Hexahedron calculation multiplier drives a wired frequency domain analysis solver to solve a frequency range of 10 GHz to 27 GHz. Because the proposed MMA can be seen as an infinitely large periodic plane, so the wave source was set to plane wave with normal incident which was opposite to the z direction, the background was set to normal, boundary condition is set to unit cell both in the x, y direction and open in the z direction. In the simulation, the principle is given as mentioned above, the absorption rate $A(\omega)$ can be derived from Equation (1).

IV. RESULTS AND DISCUSSIONS

Figure 2 shows the calculated absorption spectrum of the triple-band MMA. Obviously, when $T = 0$, $A = 1 - R$, the calculation results are almost consistent with the previous theoretical analysis. The three absorption peaks were 16.919 GHz, 21.084 GHz and 25.266 GHz at 99.90%, 97.76% and 99.18%, respectively. Compared with the multi-band MMA absorption listed in Table 1, the proposed MA this time has higher absorption rates in the K_u and K bands. Two of the peaks are above 99%, another is close to 98%. The polarization insensitivity of

the triple-band MMA is analyzed here. When the TE wave is normal incident on the surface. Electric field vector is parallel to the x -axis, and the incident wave is parallel to the z axis. The polarization angle of TE wave is the deflection angle between the electric field vector and the x -axis. The different absorption effects of MMA can be obtained by changing its angle degrees. Figure 3 shows that when the polarization angle changes, the absorption frequency and absorption rates of the absorber are almost unchanged. The performance of this study shows that the MMA is not sensitive to polarization.

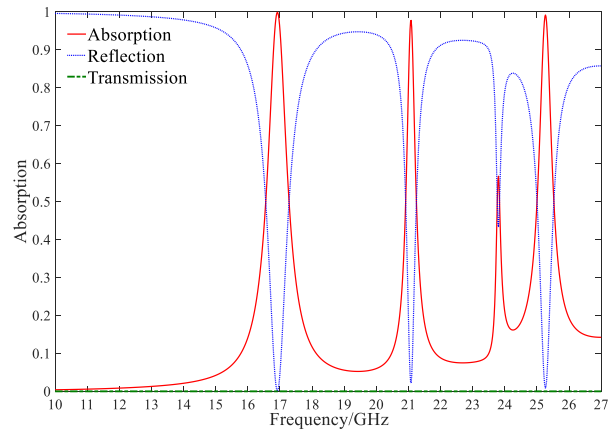


Fig. 2. Triple-band MMA's simulated absorption, reflection and transmission spectra with $p=15$ mm, $a=0.6$ mm, $b=2.0$ mm, $t_1=0.018$ mm, $t_2=1.2$ mm and $t_3=0.018$ mm.

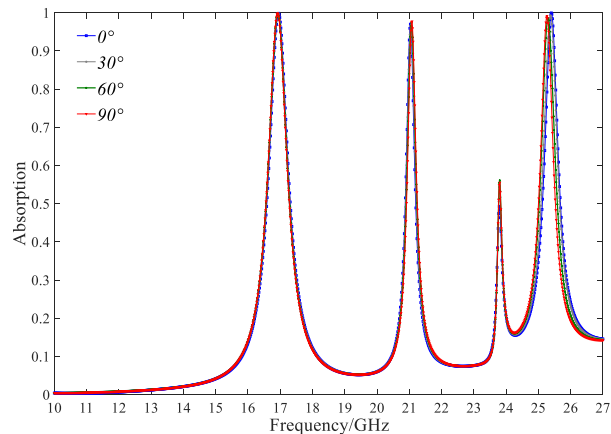


Fig. 3. Absorption spectra at different polarization angles.

The comparison of the CST and HFSS (15 GHz - 27 GHz) results is shown in Fig. 4. Because the algorithm is different, the calculation error is also different. CST is a simulator based on FDTD (Finite Difference Time Domain Method) electromagnetic field solving algorithm, and HFSS is a simulator based on FEM (Finite Element Method) electromagnetic field solving algorithm.

Different mesh partitioning accuracy and different residuals may also lead to deviation of the results, even the difference in the simulation results in the frequency domain will be more obvious. However, the absorption trend of the two groups of simulation spectra is the same, although the resonance frequency is slightly different, the peaks value are highly similar. The relative errors of absorption rate and frequency are shown in Table 1 and Table 2, respectively. The maximum relative error of frequency is only 11.07% and the lowest relative error of absorption rate can be as low as zero.

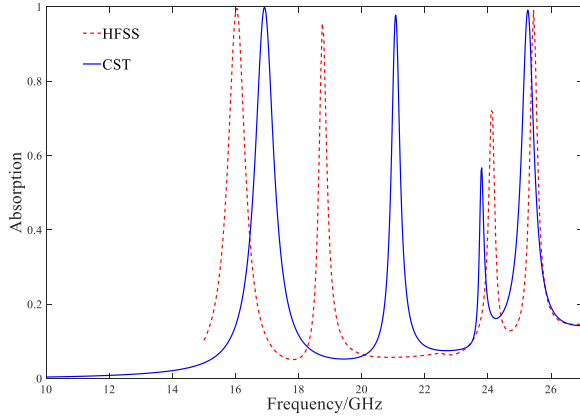


Fig. 4. Comparison of CST and HFSS absorption spectra of the proposed MA.

Table 1: The CST and HFSS simulation data for absorption rate of each resonance peak

Peaks	HFSS Absorption A_i	CST Absorption \hat{A}_i	Relative Error $= \frac{e_i}{\hat{A}_i} = \frac{A_i - \hat{A}_i}{\hat{A}_i} \times 100\%$
1	0.996	0.999	-0.3003%
2	0.9559	0.9776	-2.22%
3	0.9918	0.9918	0%

Table 2: The CST and HFSS simulation data for frequency of each resonance peak

Peaks	HFSS Frequency F_i	CST Frequency \hat{F}_i	Relative Error $= \frac{e_i}{\hat{F}_i} = \frac{F_i - \hat{F}_i}{\hat{F}_i} \times 100\%$
1	16.05 GHz	16.919 GHz	-0.3035%
2	18.75 GHz	21.084 GHz	-11.07%
3	24.45 GHz	25.266 GHz	-3.2296%

Here, the electric field, magnetic field and surface current distribution of the absorber is analyzed through the Fig. 5, Fig. 6. and Fig. 7. In the proposed unit, the

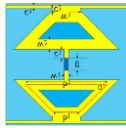

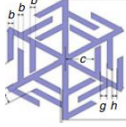
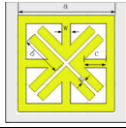
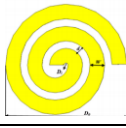
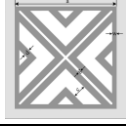

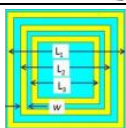
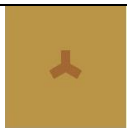
horizontal and vertical direction are electric field direction (E) and magnetic field direction (H), respectively as given by Fig. 1. In the case of a frequency of 16.919 GHz, when the electromagnetic wave incidents into the MMA, electric charges in the top three-fork star structure move in both positive and negative directions on the y -axis, clustered on the sides, and the dipole resonance is formed in this structure, as shown in Fig. 6 (a). Because the top layer is inductive with the charge in the bottom layer, from Fig. 7, that two layers form a reverse current on their respective surfaces. As shown in Fig. 6 (a), in the metamaterial structure designed in this paper, the magnetic dipole resonance is induced due to the existence of reverse current. Thus, most of the magnetic field distribution occupies the intermediate dielectric layer. At the frequency of 16.919 GHz, when the electromagnetic wave incidents into the MMA, most of the energy is consumed due to the combined action of dipole resonance and magnetic dipole resonance. Similarly, at the frequency of 21.084 GHz, due to the action of electromagnetic waves, there is a positive and negative charge aggregation on both sides of the top structure, resulting in a powerful electric field at that position, as illustrated by Fig. 5 (b). It is precisely because the opposite current accumulates on the upper and lower sides respectively that the dipole resonance is formed in the structure. The charges in the upper and lower layers of metal induce each other to generate a reverse current, thus forming a loop, as shown in Fig. 7 (b). As shown in Fig. 6 (b), the magnetic field is mainly distributed in the middle dielectric layer, which clarifies the location of magnetic resonance. Therefore, when the incident frequency of electromagnetic waves is 21.084 GHz, the coupling effect of electric dipole resonance and magnetic dipole resonance completes the loss. At the frequency of 25.266 GHz, the electromagnetic wave is incident, and the top layer and the bottom metal gather more positive and negative charges on the upper and lower sides. Because of the sensing between the charges, the electric field presents a state as shown in Fig. 5 (c), where the top layer of the structure and the bottom metal surface also generate a reverse current, as illustrated by Fig. 7 (c). It can be seen from Fig. 6 (c) that the distribution of the magnetic field concentrated in the intermediate dielectric layer is also due to the presence of magnetic resonance in the structure. Thus, by the same token, the incident electromagnetic wave is consumed at a frequency of 25.266 GHz. The structure can form electrical resonance and magnetic resonance, which can absorb the incident electromagnetic wave with higher absorption rates.

Figure 8 shows the real and imaginary parts of equivalent permittivity and permeability ($Re \epsilon(\omega)$, $Im \epsilon(\omega)$, $Re \mu(\omega)$ and $Im \mu(\omega)$) respectively, which are extracted by retrieved effective parameters. Due to $R(\omega) = |S_{11}|^2 = \left[\frac{Z(\omega)-1}{Z(\omega)+1} \right]^2$ and the impedance $Z(\omega) =$

$\sqrt{\mu/\epsilon}$, relatively perfect impedance matching is achieved at the frequencies of 16.919 GHz, 21.084 GHz and 25.266 GHz. At this point, the absorber responds to the external field, generates the opposite magnetic dipole, resulting in magnetic resonance and forming absorption peaks which were shown in the spectrum [36]. Comparing electric-field distributions at 16.919 GHz, 19.5 GHz, 21.084 GHz, 23 GHz and 25.266 GHz as shown by Fig. 5 and Fig. 9, obviously there are stronger fields at 16.919

GHz, 21.084 GHz and 25.266 GHz, Fig. 8 gives that the real and imaginary parts of the permittivity and the permeability are equal at these frequencies, that to say, the impedance at these frequencies is well matched. While at 16.919 GHz and 21.084 GHz, the real and imaginary parts of the permittivity and the permeability are not equal, which means the impedance don't match, leading to weaker electric fields. There are similar laws for magnetic-field distributions.

Table 3: Absorption rates comparison with other kinds of multi-band MMAs

Absorber	Absorption Rate	Working Frequency (GHz)	Resonance Frequency (GHz)	Structure of Top Layer	Materials	Unit Cell Size (mm ²)
Reference [28]	99.80% 97.40% 99.90%	2-16.5	4.60 8.41 14.67		Copper -FR-4- Copper	10×10
Reference [29]	95.59% 94.20%	9.5-11.5	10.15 10.50		Copper -FR-4- Copper	12×12
Reference [30]	99.00% 98.00%	8-12	9.80 10.30		Conductor -Substrate- Conductor	15×15
Reference [21]	99.00% 99.00%	4-10	6.16 7.79		Copper -FR-4- Copper	14×14
Reference [23]	99.40% 96.70% 99.10%	8-17	9.86 12.24 15.34		Copper -FR-4- Copper	18×18
Reference [31]	99.87% 99.98% 99.99%	2-10	3.07 5.65 8.11		Copper -FR-4- Copper	21.6×21.6
Reference [32]	99.16% 99.95%	4-24	5.98 11.12		Copper -FR-4- Copper	18×18
Reference [33]	99.00% 93.00% 95.00%	2-12	4.06 6.73 9.22		Copper -FR-4- Copper	20×20
The presented work	99.90% 97.76% 99.18%	10-27	16.919 21.084 25.266		Copper -FR-4- Copper	15×15

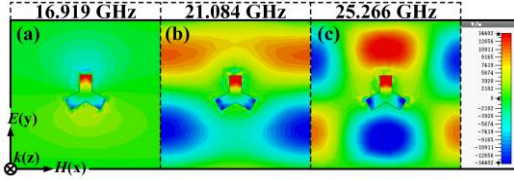


Fig. 5. Electric-field distributions of the MMA: (a) 16.919 GHz, (b) 21.084 GHz, and (c) 25.266 GHz.

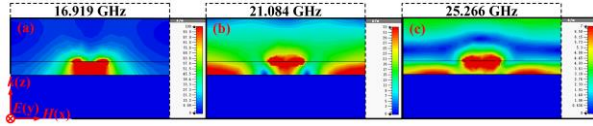


Fig. 6. Magnetic-field distributions: (a) 16.919 GHz, (b) 21.084 GHz, and (c) 25.266 GHz.

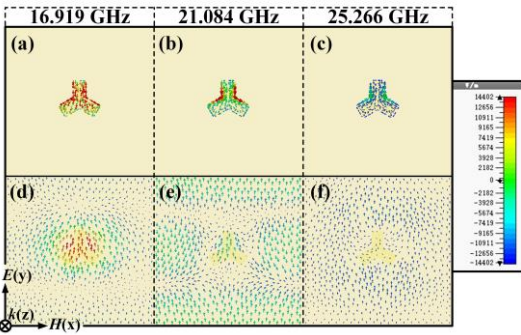


Fig. 7. Surface current distributions: (a) Top layer at 16.919 GHz, (b) top layer at 21.084 GHz, (c) top layer at 25.266 GHz, (d) bottom layer at 16.919 GHz, (e) bottom layer at 21.084 GHz, and (f) bottom layer at 25.266 GHz.

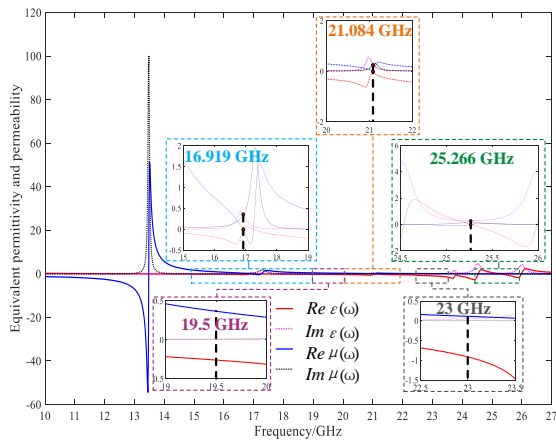


Fig. 8. Extracted electromagnetic parameters: real and imaginary parts of permittivity $Re \epsilon(\omega)$, $Im \epsilon(\omega)$ and permeability $Re \mu(\omega)$, $Im \mu(\omega)$.

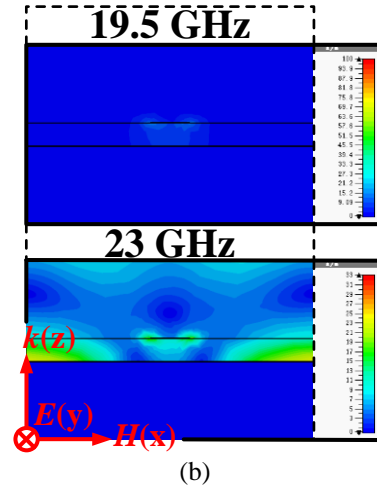
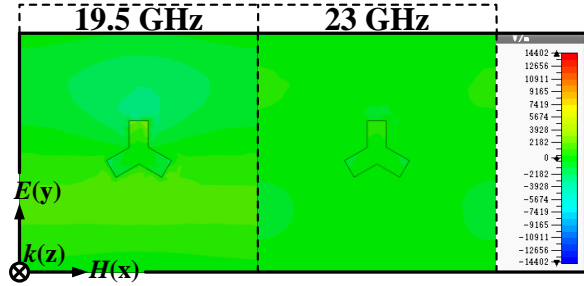


Fig. 9. Electric-field distributions: (a) and magnetic-field distributions; (b) of the MMA for 19.5 GHz and 23 GHz.

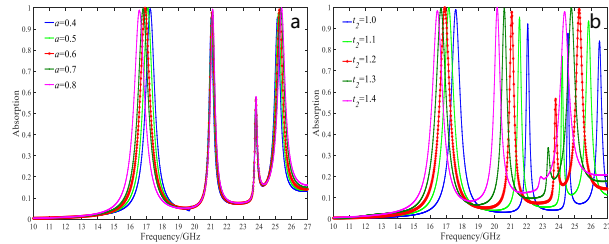


Fig. 10. Relationships of triple-band absorption spectra and geometric parameters. (a) Different line width a . (b) Different thickness t_2 of the dielectric layer.

Optimization of main geometric parameters about the structure is carried out and how key structural parameters affect the MMA absorption rate is analyzed. The effect of the parameter a on absorption rates is shown in Fig. 10 (a) and Table 4. As the parameter a increased from 0.4 mm to 0.8 mm, the three absorption peaks also changed. The absorption of the first crest increased from 0.9954 to 0.9993 and then decreased to 0.9882, and the absorption rate of the second crest gradually increased by 0.0430, while the absorption

rate of the third crest increased by 0.0446. When the absorption rate changes slightly, the central frequency corresponding to the peak is also changed, and the three frequency values are moving 0.663 GHz, 0.085 GHz and 0.255 GHz respectively. Secondly, we analyzed the effect on the absorption rates by changing the thickness of the intermediate dielectric layer t_2 , as shown in Fig. 10 (b) and Table 5. When the thickness t_2 increased from 1.0

mm to 1.4 mm by 0.1 mm step, the 1st and 3rd absorption peaks increased first and then decreased, the second peak increased gradually. The third of these peaks is relatively large, and at the same time as the corresponding frequency is moving 2.159 GHz, the peak absorption rate increases from 0.9795 to 0.9971 and eventually to 0.8409. The frequency variation values corresponding to the first two peaks are 1.139 GHz and 1.904 GHz, respectively.

Table 4: Peaks and frequencies corresponding to different line width values

a (mm)	Peak 1		Peak 2		Peak 3	
	Frequency (GHz)	Absorption	Frequency (GHz)	Absorption	Frequency (GHz)	Absorption
0.4	17.242	0.9953	21.033	0.9506	25.130	0.9552
0.5	17.089	0.9993	21.050	0.9671	25.198	0.9769
0.6	16.919	0.9990	21.084	0.9776	25.266	0.9918
0.7	16.800	0.9949	21.101	0.9874	25.334	0.9980
0.8	16.579	0.9882	21.118	0.9935	25.385	0.9998

Table 5: Peaks and frequencies corresponding to thickness values of different dielectric layers

t_2 (mm)	Peak 1		Peak 2		Peak 3	
	Frequency (GHz)	Absorption	Frequency (GHz)	Absorption	Frequency (GHz)	Absorption
1.0	17.599	0.9891	20.207	0.9214	26.524	0.8408
1.1	17.174	0.9987	20.560	0.9534	25.844	0.9353
1.2	16.919	0.9990	21.084	0.9976	25.266	0.9918
1.3	16.681	0.9938	20.608	0.9937	24.773	0.9971
1.4	16.460	0.9833	20.166	0.9986	24.365	0.9795

V. CONCLUSION

A novel triple-band MMA has been designed in the microwave range, and its polarization insensitivity is verified. From the calculational results, it can be seen the MMA has three absorption peaks at 16.919 GHz, 21.084 GHz and 25.266 GHz frequencies, with absorption rates of 0.9990, 0.9776 and 0.9918, respectively. Combined with the absorption mechanism, the absorption characteristics are attributed to the electromagnetic coupling that exists between structures. The shape dimensions of the top metal structure and the thickness of the intermediate dielectric layer both have an effect on absorption performance, but the effect of the change of polarization angle is not obvious, so its polarization insensitivity is verified. When the line width a increases from 0.4 mm to 0.8 mm, the change of three peaks is not obvious, the first increases by 0.0111 and then decreases by 0.0039, and the second third increases by 0.0430 and 0.0446 respectively, while the frequency in which it is located has increased to varying degrees. In the process of increasing the thickness of dielectric layer from 1.0 mm to 1.4 mm, the simulation results show that the change has the greatest influence on the third absorption peak, and the value of its frequency forward movement reaches 2.159 GHz. Compared with the previous reports, the proposed MMA presents a greater practical feasibility

in term of low-frequency microwave and polarization-insensitivity, especially all three peak absorption rates are close to 100%, in addition, it has important value in the fields of thermal radiation measuring instrument, spectrum imaging detector and electromagnetic wave modulator.

ACKNOWLEDGMENT

This work is supported by National Natural Science Foundation of China (Grant No 51775237), Key R&D Projects of the Ministry of Science and Technology of China (Grant Nos. 2018YFB1107600 and 2017YFA0701200), Key scientific research project of Jilin Provincial Department of Education (Grant No. JJKH20200972KJ) and Key Projects of Jilin Province Science and Technology Development Plan (Grant No. 20200401121GX) of China.

REFERENCES

- [1] V. G. Veselago, "The electrodynamics of substances with simultaneously negative values of ϵ and μ ," *Soviet Physics Uspekhi*, vol. 10, no. 4, pp. 509-514, 1968.
- [2] R. A. Shelby, D. R. Smith, and S. Schultz, "Experimental verification of a negative index of refraction," *Science*, vol. 292, no. 5514, pp. 77-79,

- Apr. 2001.
- [3] N. I. Landy, S. Sajuyigbe, J. J. Mock, D. R. Smith, and W. J. Padilla, "Perfect metamaterial absorber," *Physical Review Letters*, vol. 100, no. 20, May 2008.
- [4] S. Maci, "A cloaking metamaterial based on an inhomogeneous linear field transformation," *IEEE T. Antenn. Propag.*, vol. 58, no. 4, pp. 1136-1143, Apr. 2010.
- [5] C. P. Scarborough, Z. H. Jiang, D. H. Werner, C. Rivero-Baleine, and C. Drake, "Experimental demonstration of an isotropic metamaterial super lens with negative unity permeability at 8.5 MHz," *Appl. Phys. Lett.*, vol. 101, no. 1, July 2012.
- [6] M. Bakir, M. Karaaslan, E. Unal, O. Akgol, and C. Sabah, "Microwave metamaterial absorber for sensing applications," *Opto.-Electron. Rev.*, vol. 25, no. 4, pp. 318-325, Dec. 2017.
- [7] C. Chen, Y. P. Sheng, and W. Jun, "Computed a multiple band metamaterial absorber and its application based on the figure of merit value," *Opt. Commun.*, vol. 406, pp. 145-150, Jan. 2018.
- [8] N. I. Landy, C. M. Bingham, T. Tyler, N. Jokerst, D. R. Smith, and W. J. Padilla, "Design, theory, and measurement of a polarization-insensitive absorber for terahertz imaging," *Phys. Rev. B*, vol. 79, no. 12, Mar. 2009.
- [9] C. Sabah, M. D. Thomson, F. Z. Meng, S. Tzanova, and H. G. Roskos, "Terahertz propagation properties of free-standing woven-steel-mesh metamaterials: Pass-bands and signatures of abnormal group velocities," *J. Appl. Phys.*, vol. 110, no. 6, Sep. 2011.
- [10] C. Sabah, F. Dincer, M. Karaaslan, E. Unal, O. Akgol, and E. Demirel, "Perfect metamaterial absorber with polarization and incident angle independencies based on ring and cross-wire resonators for shielding and a sensor application," *Opt. Commun.*, vol. 322, no. 322, pp. 137-142, July 2014.
- [11] H. Tao, N. I. Landy, C. M. Bingham, X. Zhang, R. D. Averitt, and W. J. Padilla, "A metamaterial absorber for the terahertz regime: Design, fabrication and characterization," *Optics Express*, vol. 16, no. 10, pp. 7181-7188, May 2008.
- [12] Y. Avitzour, Y. A. Urzhumov, and G. Shvets, "Wide-angle infrared absorber based on a negative-index plasmonic metamaterial," *Phys. Rev. B*, vol. 79, no. 4, Jan. 2009.
- [13] Y. Z. Cheng, H. L. Yang, Z. Z. Chen, and N. Wu, "Perfect metamaterial absorber based on a split-ring-cross resonator," *Appl. Phys. a-Mater.*, vol. 102, no. 1, pp. 99-103, Jan. 2011.
- [14] J. M. Hao, L. Zhou, and M. Qiu, "Nearly total absorption of light and heat generation by plasmonic metamaterials," *Phys. Rev. B*, vol. 83, no. 16, Apr. 2011.
- [15] F. Alves, B. Kearney, D. Grbovic, N. V. Lavrik, and G. Karunasiri, "Strong terahertz absorption using SiO₂/Al based metamaterial structures," *Appl. Phys. Lett.*, vol. 100, no. 11, Mar. 2012.
- [16] Q. Y. Wen, Y. S. Xie, H. W. Zhang, Q. H. Yang, Y. X. Li, and Y. L. Liu, "Transmission line model and fields analysis of metamaterial absorber in the terahertz band," *Optics Express*, vol. 17, no. 22, pp. 20256-20265, Oct. 2009.
- [17] J. P. Zhong, Y. J. Huang, G. J. Wen, H. B. Sun, P. Wang, and O. Gordon, "Single-/dual-band metamaterial absorber based on cross-circular-loop resonator with shorted stubs," *Appl. Phys. a-Mater.*, vol. 108, no. 2, pp. 329-335, Aug. 2012.
- [18] H. M. Lee and J. C. Wu, "A wide-angle dual-band infrared perfect absorber based on metal-dielectric-metal split square-ring and square array," *J. Phys. D. Appl. Phys.*, vol. 45, no. 20, May 2012.
- [19] Y. Ma, Q. Chen, J. Grant, S. C. Saha, A. Khalid, and D. R. S. Cumming, "A terahertz polarization insensitive dual band metamaterial absorber," *Optics Letters*, vol. 36, no. 6, pp. 945-947, Mar. 2011.
- [20] Y. H. Zhao, Q. Z. Hao, Y. Ma, M. Q. Lu, B. X. Zhang, M. Lapsley, I. C. Khoo, and T. J. Huang, "Light-driven tunable dual-band plasmonic absorber using liquid-crystal-coated asymmetric nanodisk array," *Appl. Phys. Lett.*, vol. 100, no. 5, Jan. 2012.
- [21] L. Li, Y. Yang, and C. H. Liang, "A wide-angle polarization-insensitive ultra-thin metamaterial absorber with three resonant modes," *J. Appl. Phys.*, vol. 110, no. 6, Sep. 2011.
- [22] Y. Ozturk and A. E. Yilmaz, "Multiband and perfect absorber with circular fishnet metamaterial and its variations," *Applied Computational Electromagnetics Society Journal*, vol. 31, no. 12, Dec. 2016.
- [23] X. J. Huang, H. L. Yang, S. Q. Yu, J. X. Wang, M. H. Li, and Q. W. Ye, "Triple-band polarization-insensitive wide-angle ultra-thin planar spiral metamaterial absorber," *J. Appl. Phys.*, vol. 113, no. 21, June 2013.
- [24] E. Delihanlar and A. H. Yuzer, "Wearable textile fabric based 3D metamaterials absorber in X-band," *Applied Computational Electromagnetics Society Journal*, vol. 35, no. 2, Feb. 2020.
- [25] J. X. Su, C. Y. Kong, Z. R. Li, X. J. Yuan, and Y. Q. Yang, "Ultra-wideband and polarization-insensitive RCS reduction of microstrip antenna using polarization conversion metasurface," *Applied Computational Electromagnetics Society Journal*, vol. 32, no. 6, pp. 524-530, June 2017.
- [26] J. Q. Wang, C. Z. Fan, P. Ding, J. N. He, Y. G.

- Cheng, W. Q. Hu, G. W. Cai, E. J. Liang, and Q. Z. Xue, "Tunable broad-band perfect absorber by exciting of multiple plasmon resonances at optical frequency," *Optics Express*, vol. 20, no. 14, pp. 14871-14878, July 2012.
- [27] F. Ding, Y. X. Cui, X. C. Ge, Y. Jin, and S. L. He, "Ultra-broadband microwave metamaterial absorber," *Appl. Phys. Lett.*, vol. 100, no. 10, Mar. 2012.
- [28] J. P. Xu, J. Y. Wang, R. C. Yang, J. P. Tian, X. W. Chen, and W. M. Zhang, "Frequency-tunable metamaterial absorber with three bands," *Optik*, vol. 172, no. 172, pp. 1057-1063, Nov. 2018.
- [29] T. T. Nguyen and S. Lim, "Bandwidth-enhanced and wide-angle-of-incidence metamaterial absorber using a hybrid unit cell," *Sci. Rep.-Uk*, vol. 7, no. 1, Nov. 2017.
- [30] J. Lee and S. Lim, "Bandwidth-enhanced and polarisation-insensitive metamaterial absorber using double resonance," *Electron. Lett.*, vol. 47, no. 1, pp. 8-U20, Jan. 2011.
- [31] B. R. Bian, S. B. Liu, S. Y. Wang, X. K. Kong, H. F. Zhang, B. Ma, and H. Yang, "Novel triple-band polarization-insensitive wide-angle ultra-thin microwave metamaterial absorber," *J. Appl. Phys.*, vol. 114, no. 19, Nov. 2013.
- [32] O. T. Gunduz and C. Sabah, "Polarization angle independent perfect multiband metamaterial absorber and energy harvesting application," *J. Comput. Electron.*, vol. 15, no. 1, pp. 228-238, Mar. 2016.
- [33] X. P. Shen, T. J. Cui, J. M. Zhao, H. F. Ma, W. X. Jiang, and H. Li, "Polarization-independent wide-angle triple-band metamaterial absorber," *Optics Express*, vol. 19, no. 10, pp. 9401-9407, May 2011.
- [34] D. R. Smith, S. Schultz, P. Markos, and C. M. Soukoulis, "Determination of effective permittivity and permeability of metamaterials from reflection and transmission coefficients," *Phys. Rev. B*, vol. 65, no. 19, May 2002.
- [35] D. R. Smith, D. C. Vier, T. Koschny, and C. M. Soukoulis, "Electromagnetic parameter retrieval from inhomogeneous metamaterials," *Phys. Rev. E*, vol. 71, no. 3, May 2005.
- [36] P. V. Tuong, J. W. Park, J. Y. Rhee, K. W. Kim, H. Cheong, W. H. Jang, and Y. P. Lee, "Symmetric metamaterials based on flower-shaped structure," *Materials Chemistry and Physics*, vol. 141, no. 1, pp. 535-539, Aug. 2013.



Han Wu was born in Jilin Province, China, in 1993. He received the B.E. degrees in Mechanical Design, Manufacturing and Automation from Changchun University of Science and Technology, Changchun, China, in 2016. Now he is a Ph.D. candidate in Metamaterial Absorber Designing and Electromagnetic Metamaterial studying at Jilin University of China.



Shijun Ji was born in Shaanxi Province, China, in 1978. He received the Ph.D. degree in Mechanical Manufacturing and Automation from Harbin Institute of Technology, Harbin, China, in 2008. He is currently a Professor at Institute of Intelligent Precision Manufacturing of Jilin University, Changchun, China. His current research interests include design and manufacturing of metamaterial absorbers, design and machining of optical components.



Ji Zhao was born in Jilin Province, China, in 1959. He received B.E. degree, M.E. degree and Ph.D. degree from the Department of Mechanical Manufacturing and Automation, Jilin University, in 1982, 1984 and 1994, respectively. He is currently a Professor at Institute of Intelligent Precision Manufacturing of Jilin University, Changchun, China. His main current research interests include design, analysis and manufacturing of complex components such as Metamaterial absorbers, Optical devices and Moulding dies.



Zhiyou Luo was born in Chongqing, China, in 1996. He received B.E. degree from the College of Biological and Agricultural Engineering, Jilin University, in 2019. Now he is a graduate student in the School of Mechanical and Aerospace Engineering, Jilin University. His mainly research interests include design of metamaterial absorbers, analysis of absorption mechanism, and electromagnetic absorption theory.



Handa Dai was born in Jilin Province, China, in 1968. He received B.E. degree, M.E. degree from the School of Mechanical Science and Engineering, Jilin University, in 1993 and 1999, and Ph.D. degree from the College of Materials Science and Engineering, Jilin University, in 2005. Now he is an Assistant Professor at Institute of Intelligent Precision Manufacturing of Jilin University. His mainly research interests include analysis about absorption mechanism of metamaterials and electromagnetic wave absorbing theory.